Supporting Information

LSPR-enhanced photocatalytic N_2 fixation over Z-scheme POMOF-derived Cu/WO_2 modified C-BiOBr with multiple active sites

Xue Yang, Donghui Cui, Tingting Zhang, Yu Liu, Fengyan Li*

Key Laboratory of Polyoxometalate and Reticular Material Chemistry of Ministry of Education, College of Chemistry, Northeast Normal University, Changchun 130024, P. R. China

Email address: lify525@nenu.edu.cn

Experimental section

1 Materials

Bismuth nitrate pentahydrate (Bi $(NO_3)_3 \cdot 5H_2O$, 99%), polyvinylpyrrolidone (PVP), glucose ($C_6H_{12}O_6 \cdot H_2O$), copper acetate monohydrate ($C_4H_6CuO_4 \cdot H_2O$, 99%), phosphotungstic acid ($H_3PW_{12}O_{40} \cdot xH_2O$), 1,3,5-benzenetricarboxylic acid ($C_9H_6O_6$, 98%), ethylene glycol (EG) and anhydrous ethanol were purchased from Sinopharm Chemical Reagent Co. Cetyltrimethylammonium bromide (CTAB, 99%), L-glutamic acid ($C_5H_9NO_4$, 99%) were purchased from Aladdin Chemical Reagent Co. The experimental water was deionized water (DI).

2 Determination of NH_3

The NH_4^+ production was determined spectrophotometrically using Nessler's reagent [1]. Nessler's reagent was purchased from Aladdin Chemical Reagents Ltd. Potassium sodium tartrate ($KNaC_4H_6O_6$) was added to minimize the interference of other ions (Fe^{3+}, Ca^{2+}, Mg^{2+}, Cr^{3+}, Ag^+, S^{2-} etc.). 25 g of $KNaC_4H_6O_6$ and 50 mL of deionized water were added to a distillation flask and sonicated for 30 min to form a homogeneous solution, then 0.5 mL of 5 moles/liter sodium hydroxide solution was added, and about 20-30% of the original volume of solvent was evaporated by heating at 110°C. The solution was then cooled to room temperature and fixed to a volume in a 50 mL volumetric flask to prepare it for use. A calibrated concentration-absorbance curve of standard ammonia solution was obtained using 5 ml of gradient concentration of ammonium chloride solution, 0.1 mL of $KNaC_4H_6O_6$ solution and 0.1 mL of Nessler's reagent (Fig. S1). The absorbance value of the fitted curve ($y = 2.7797 x + 0.0167$, $R^2 = 0.9999$) showed a good linear relationship with the ammonia concentration. Ammonia production from the synthesized photocatalysts was detected by mixing 5 mL of centrifugally filtered reaction solution with 0.1 mL of $KNaC_4H_6O_6$ solution and 0.1 mL of Nessler's reagent under dark conditions for 15 min and then detected by UV-visible spectrophotometer at 420 nm.

3 Determination of N_2H_4

The hydrazine content in the solution after photocatalysis was determined by Watt's and Crisp's methods [2]. The color developer was prepared by dissolving p-dimethylaminobenzaldehyde and hydrochloric acid in ethanol. Hydrazine standard solution of gradient concentration was mixed with the color developer to obtain the standard curve. Then 2 mL of the colorant was added into 2 mL of centrifugal reaction solution, which was allowed to stand for 20 min and then detected by UV-visible spectrophotometer at 460 nm.

4 N_2 temperature-programmed desorption (N_2-TPD)

100 mg of catalyst was placed in a u-shaped quartz tube and He gas flow was pretreated to 300 °C at a ramp rate of 10 °C/min, preheated at a flow rate of 50 mL/min for 1 h, and then cooled to 50 °C. After pretreatment, feed N_2 was passed and adsorbed to saturation at 25 °C at a flow rate of 50 mL/min. Then, the physical adsorption of N_2 was removed by He flow (50 mL min^{-1}) at 50 °C for 1 h. The catalyst was then passed through the catalyst at a flow rate of 50 mL/min for 1 h to remove the N_2 physically adsorbed. Finally, the catalyst was heated at a rate of 10 C min^{-1} from 50 °C to 600 °C. An on-line analytical heat transfer detector (TPD, microcrystalline AutoChem II 2920) was used.

5 Inductively coupled plasma atomic emission spectroscopy (ICP-AES)

5 mg of the sample was dissolved in 5 ml of aqua regia, stirred for 30 minutes and kept in an oven at 100° C for 6 hours. The cooled solution was filtered and fixed in a 25 ml volumetric flask for testing.

6 Electrochemical tests

Electrochemical testing was performed using a CHI661D electrochemical workstation. The light source was a 300 W xenon lamp with an AM1.5 filter and a >700 nm visible cut-off filter. The working electrode was a photocatalytic material, the reference electrode was $Hg/HgCl_2$ and the counter electrode was a platinum foil. Typically, 50 mg of sample, 100 mg of geraniol and 5 mg of ethyl cellulose were

thoroughly mixed with 5 ml of ethanol in an onyx mortar and then uniformly covered on the FTO glass sheet as the working electrode. The photoelectric properties of these materials were studied using 0.5 M Na_2SO_4 aqueous solution as the electrolyte solution.

7 DFT calculations

The first-principles calculations are performed using the framework of density functional theory (DFT) within the Vienna Ab-initio simulation package (VASP) [3]. The exchange-correlation interaction was processed using a generalized gradient approximation (GGA) in the form of Perdew-Burke-Ernzerhof (PBE) [4]. The thickness of the vacuum layer in the Z-direction was fixed at 20 Å using IOPTCELL to avoid the effect of interactions between adjacent fragments. The kinetic energy cutoff of the plane wave used to extend the Kohn-Sham electron wave function was set to 450 eV. The iterative convergence of energy is 10^{-5} eV. All atoms were allowed to relax until the Hellmann-Feynman force was less than 0.01 eV/Å. The Brillouin zone was sampled by a 3 × 2 × 1 k-point grid for C-BOB and Cu/WO_2/C-BOB. The change in Gibbs free energy (ΔG) of NRR intermediates was calculated using

$$\Delta G = \Delta E + \Delta ZPE - T\Delta S$$

Where ΔE is the energy change at each step of the reaction, ΔZPE is the zero point energy, T is the temperature (298.15 K), and ΔS is the change of entropy. The ΔZPE was calculated by using the vibrational frequency of intermediates. The corrected values of the free energy are calculated by VASPKIT, a plug-in for VASP.

8 Apparent quantum efficiency (AQE) calculation

Photocatalytic experiments to calculate AQE were carried out in a photocatalytic double-layer quartz bottle reactor. The catalyst mass, solution volume, reaction time, and simulated solar irradiation area were 10 mg, 100 mL, 1 h, and 30 cm^2 respectively. The monochromatic filters of 420 nm was used to filter the light. The AQE was calculated through the following equation:

$$AQE = \frac{N_e}{N_P} = \frac{6 \times N_{NH3}}{N_p} = \frac{6 \times n_{NH3} \times N_A}{\frac{P \times S \times t}{hv}} \times 100\%$$

Where, N_e, N_p and N_{NH3} represent the number of reacted electrons, incident photons, and generated NH_3, respectively; N_A was Avogadro's constant; h was Planck's constant; P, S, and t were the incident light intensity, irradiated area, and reaction time respectively.

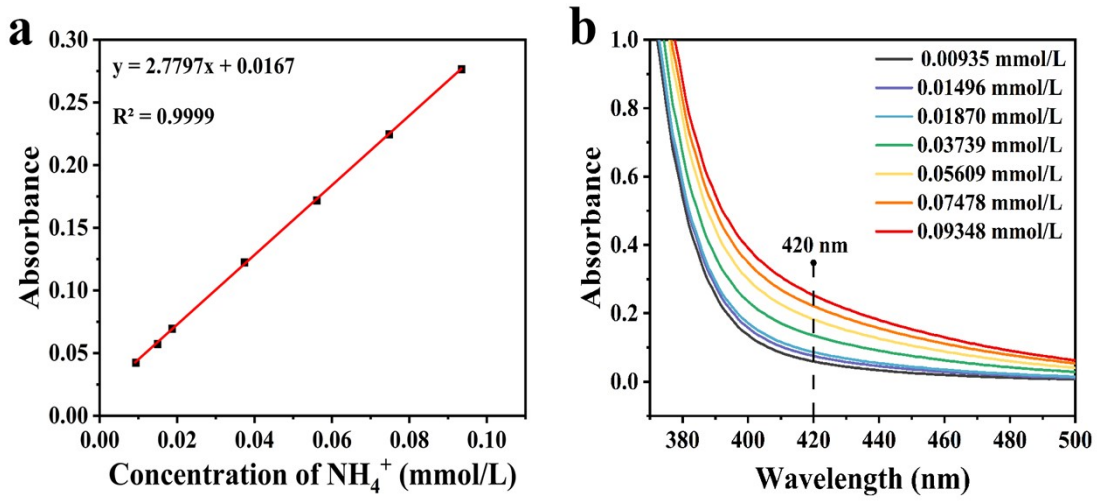

Fig. S1. Standard curves for NH_4^+ with Nessler's reagent.

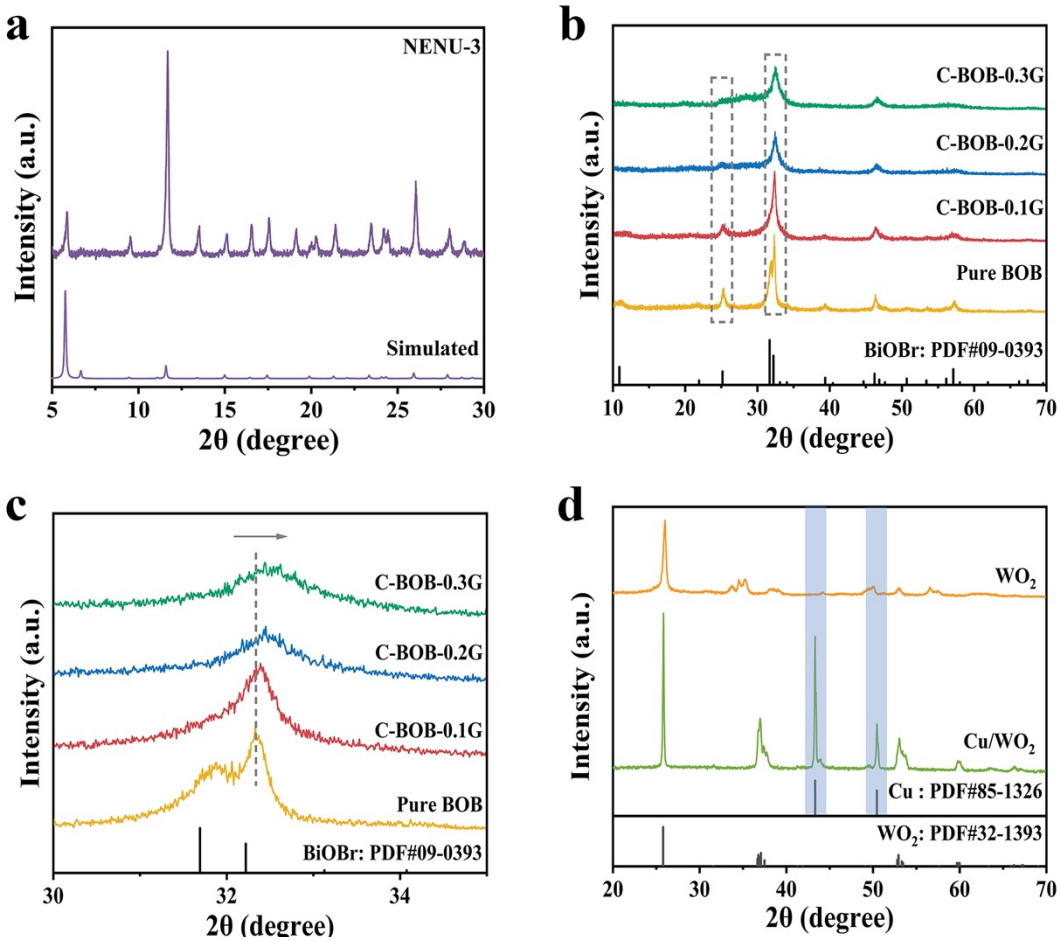

Fig. S2. (a) XRD spectra of NENU-3. (b, c) XRD spectra of C-BOB samples with different glucose additions. (d) XRD spectra of WO_2 and Cu/WO_2.

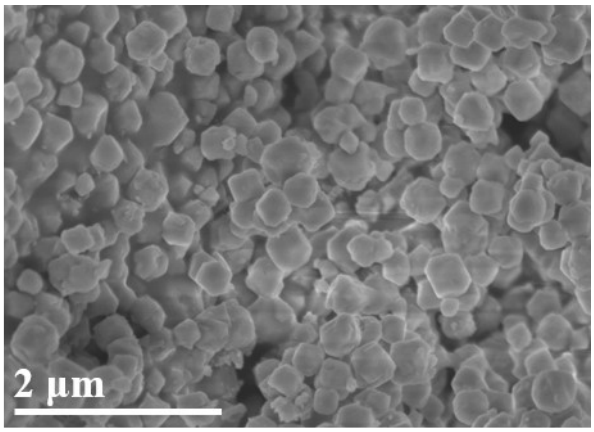

Fig. S3. SEM image of NENU-3.

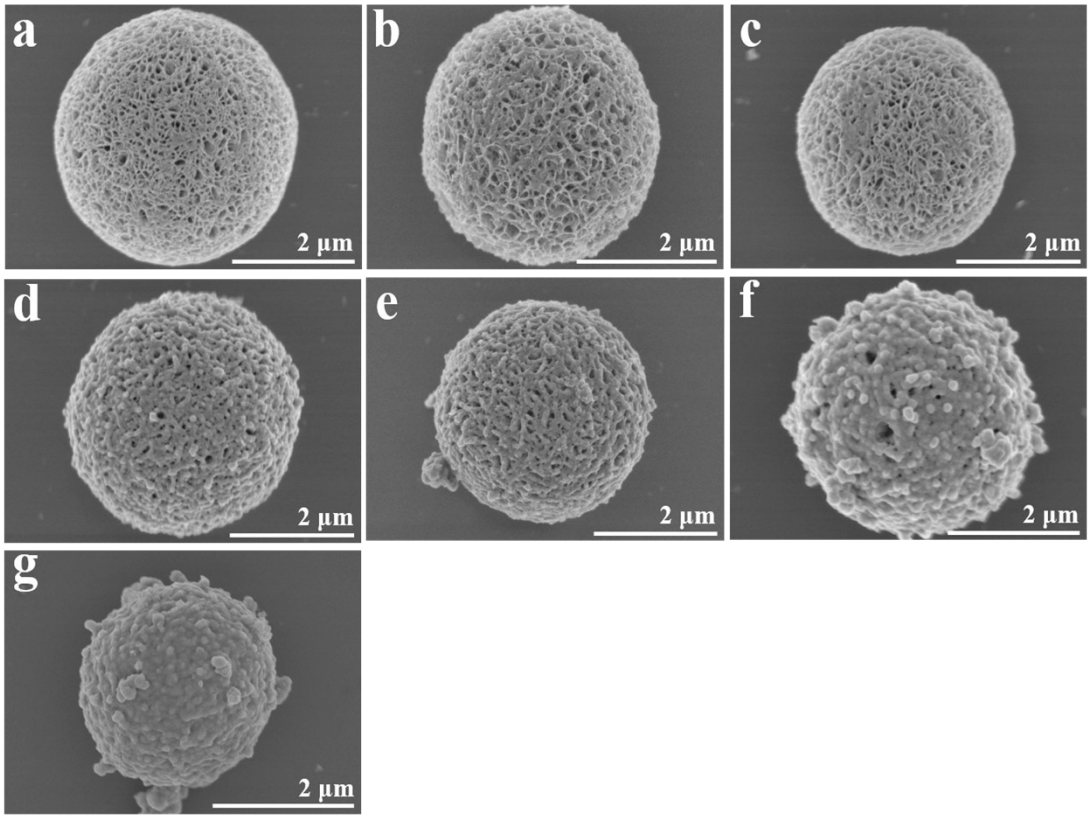

Fig. S4. SEM images of Cu/WO_2/C-BOB-x (x being the mass fraction ratio of Cu/WO_2 doping).

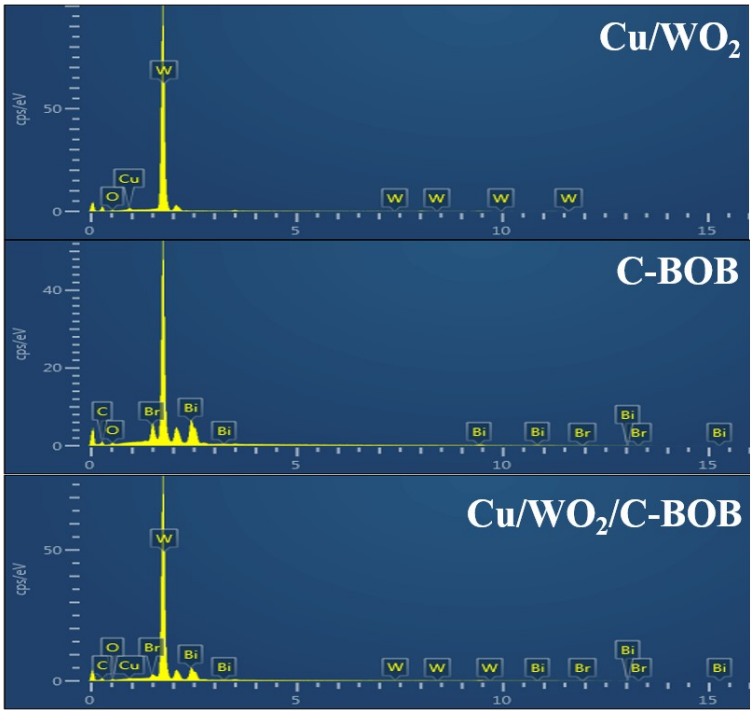

Fig. S5. Energy-dispersive X-ray (EDX) spectrum of samples.

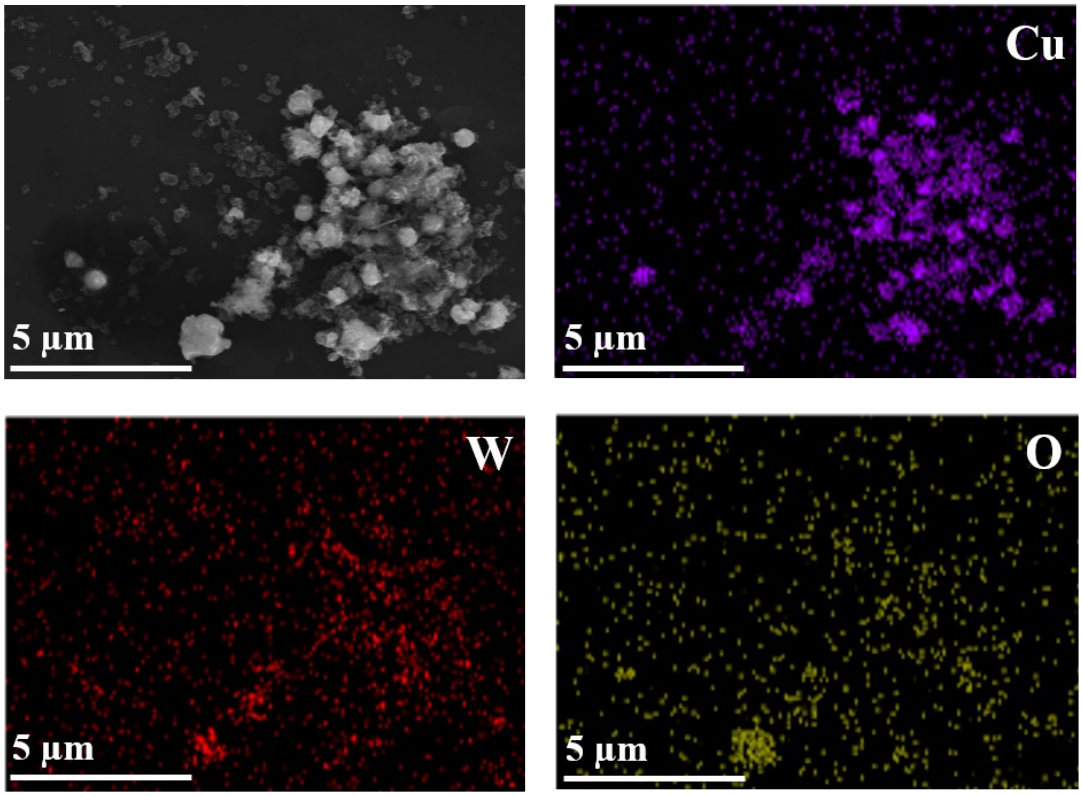

Fig. S6. Elemental mapping of Cu/WO_2.

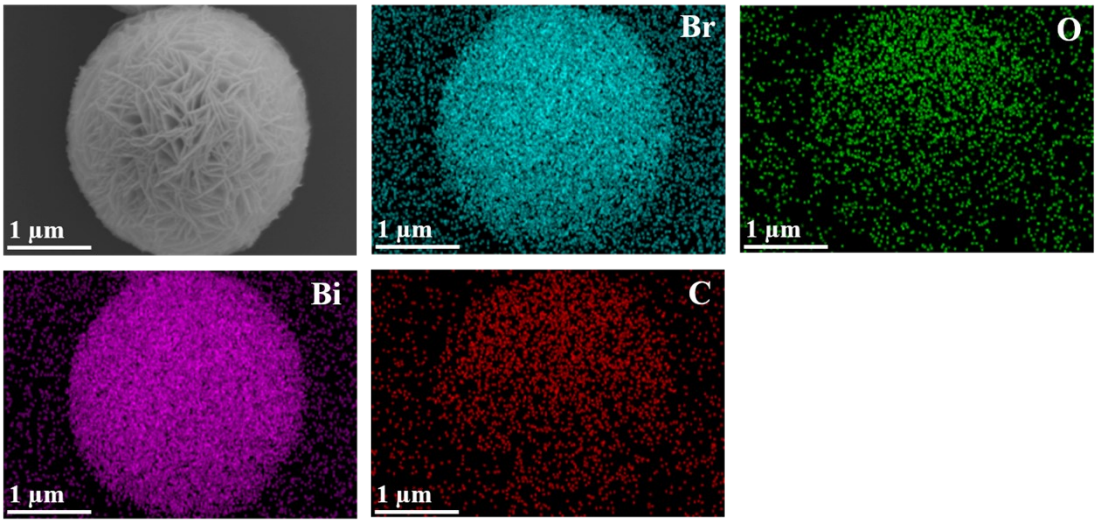

Fig. S7. Elemental mapping of C-BOB.

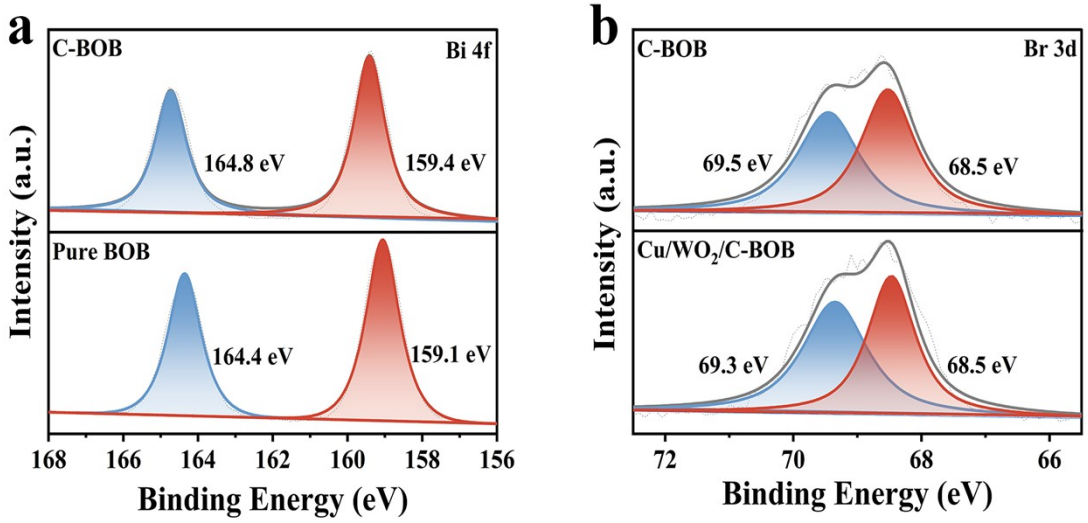

Fig. S8. (a) High-resolution XPS spectra of the Bi 4f peaks of Pure BOB and C-BOB. (b) High-resolution XPS spectra of the Br 3d peaks of C-BiOBr and Cu/WO_2/C-BiOBr.

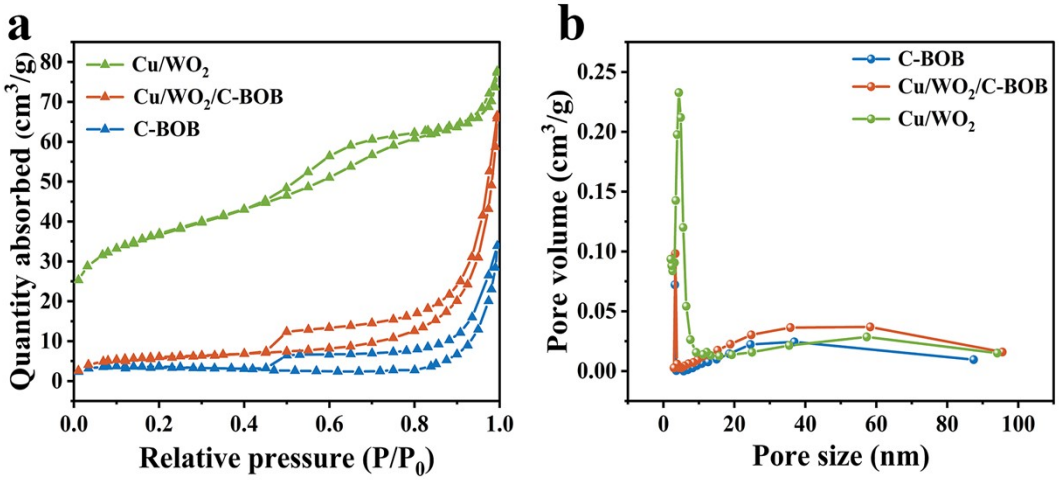

Fig. S9. (a) Nitrogen adsorption/ desorption isotherms and (b) pore size distribution of samples.

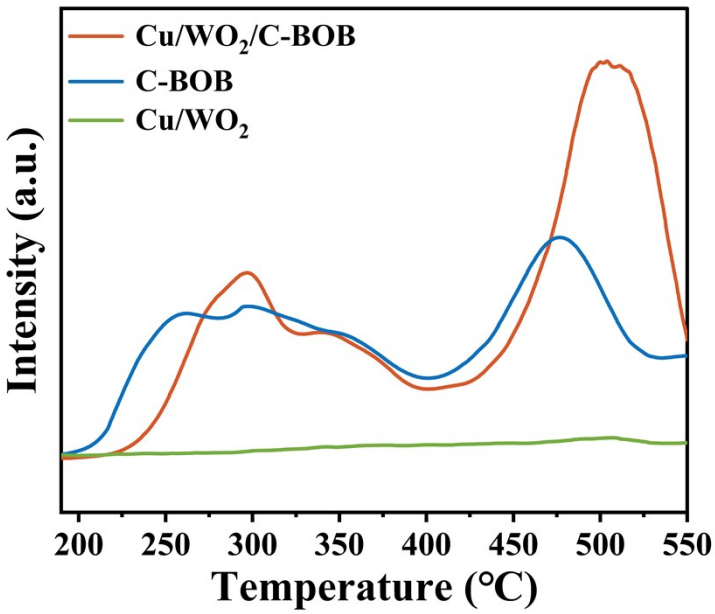

Fig. S10. N_2-TPD profiles of Cu/WO_2、C-BOB and Cu/WO_2/C-BOB.

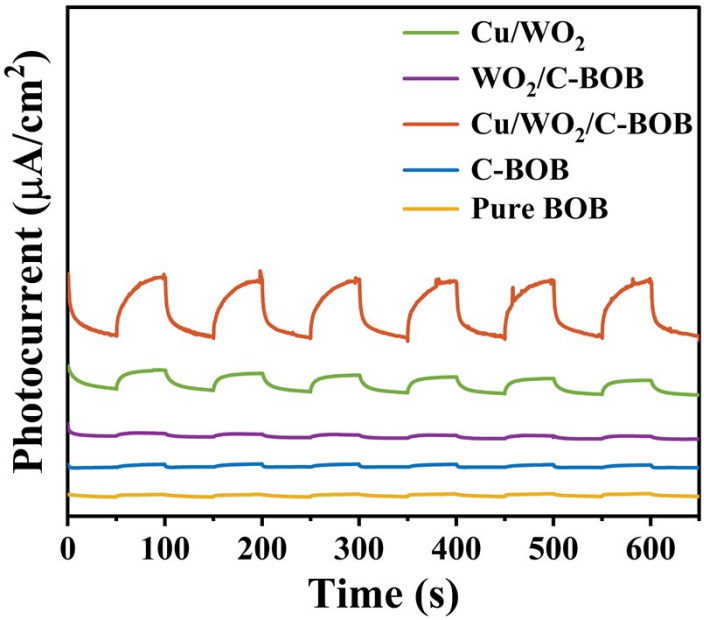

Fig. S11. Transient photocurrent responses of samples (λ > 700 nm).

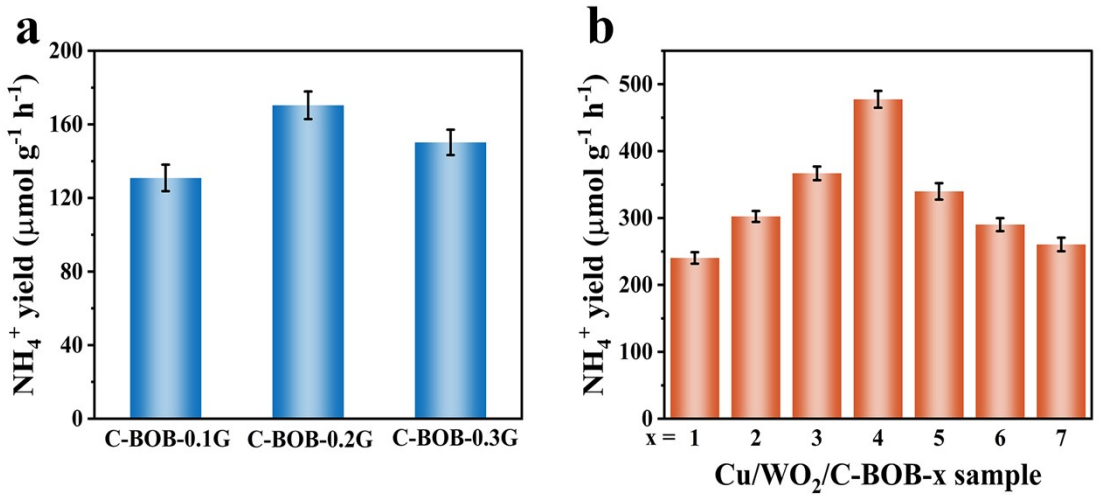

Fig. S12. (a) Yields of NH_4^+ from C-BOB samples with different glucose additions. (b) Yields of NH_4^+ from Cu/WO_2/C-BOB-x (x being the mass fraction ratio of Cu/WO_2 doping).

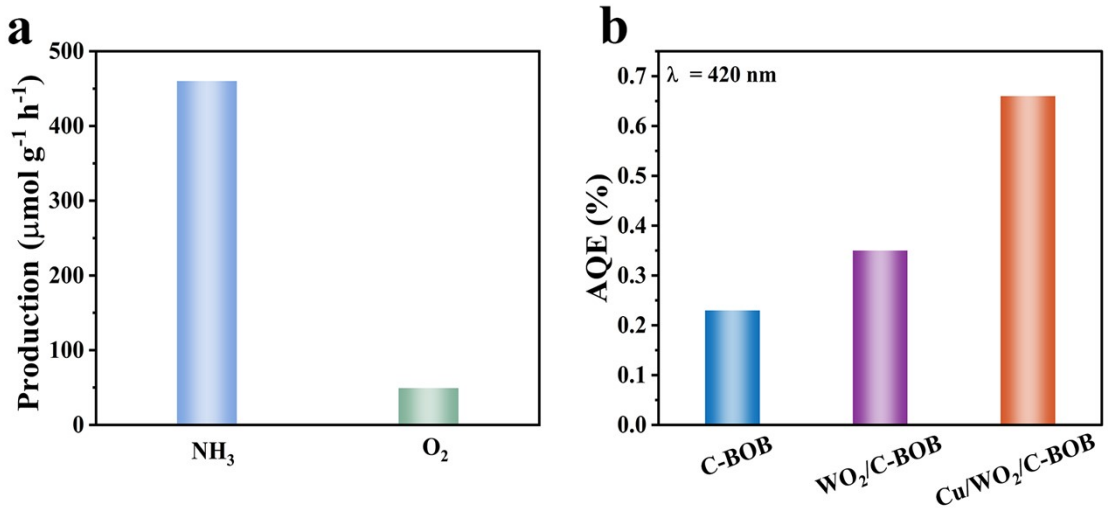

Figure S13. (a) NH_3 and O_2 production of Cu/WO_2/C-BOB. (b) The apparent quantum efficiency of different samples at a wavelength of 420 nm.

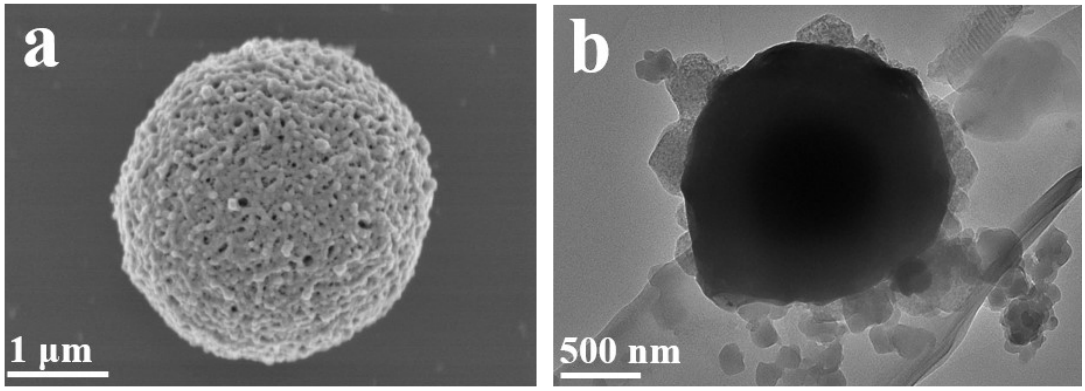

Fig. S13. (a) SEM and (b) TEM images of Cu/WO_2/C-BOB after cycling experiments.

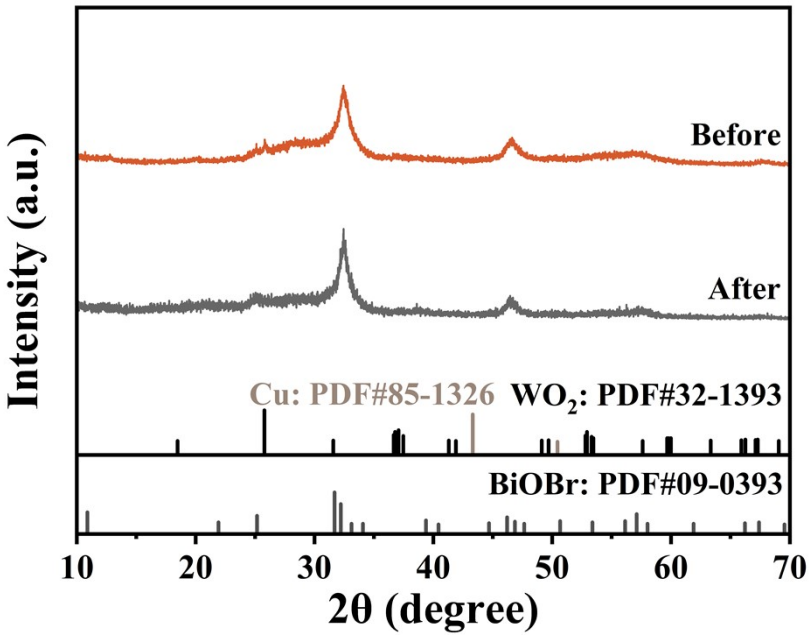

Fig. S14. XRD images of Cu/WO_2/C-BOB before and after cycling experiments.

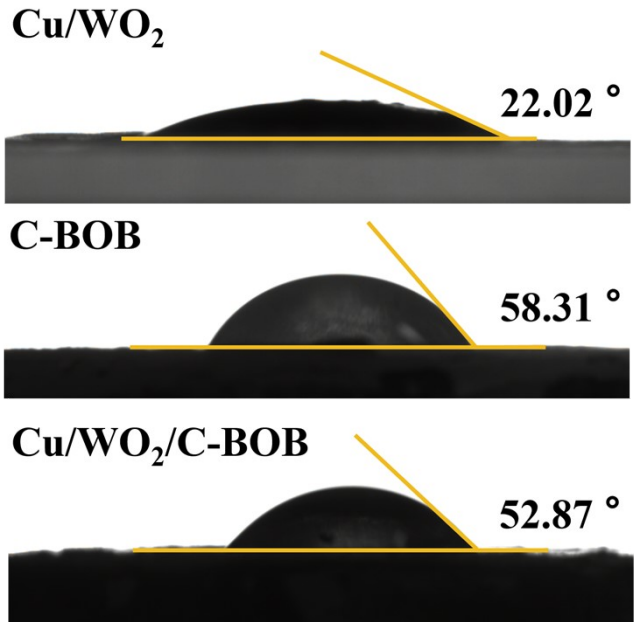

Fig. S15. Static water contact-angle measurement of Cu/WO_2、C-BOB and Cu/WO_2/C-BOB.

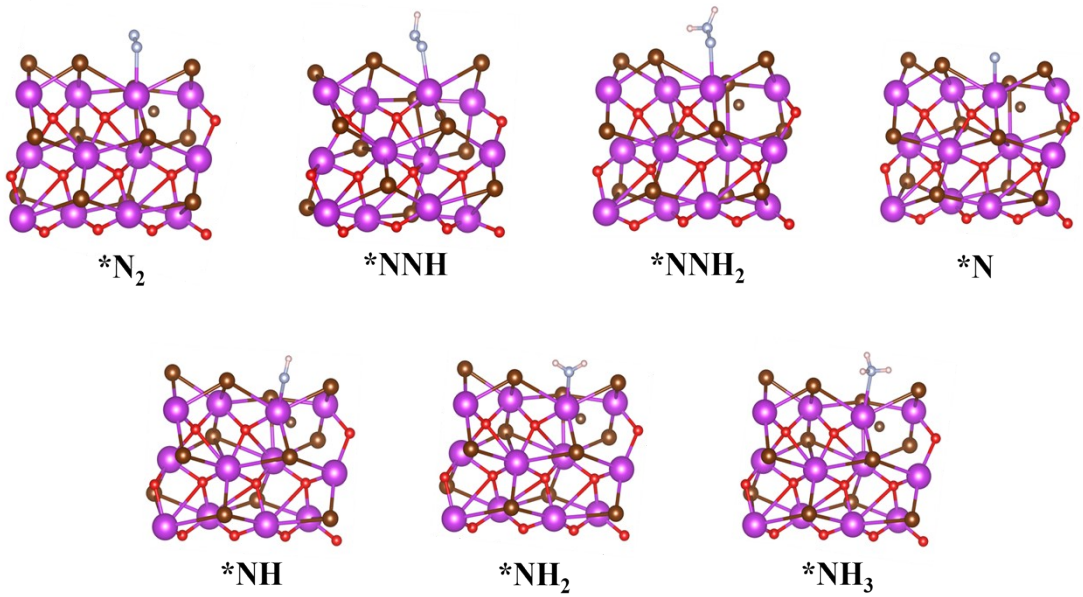

Fig. S16. The adsorption diagrams of the N_2 fixation process over C-BOB.

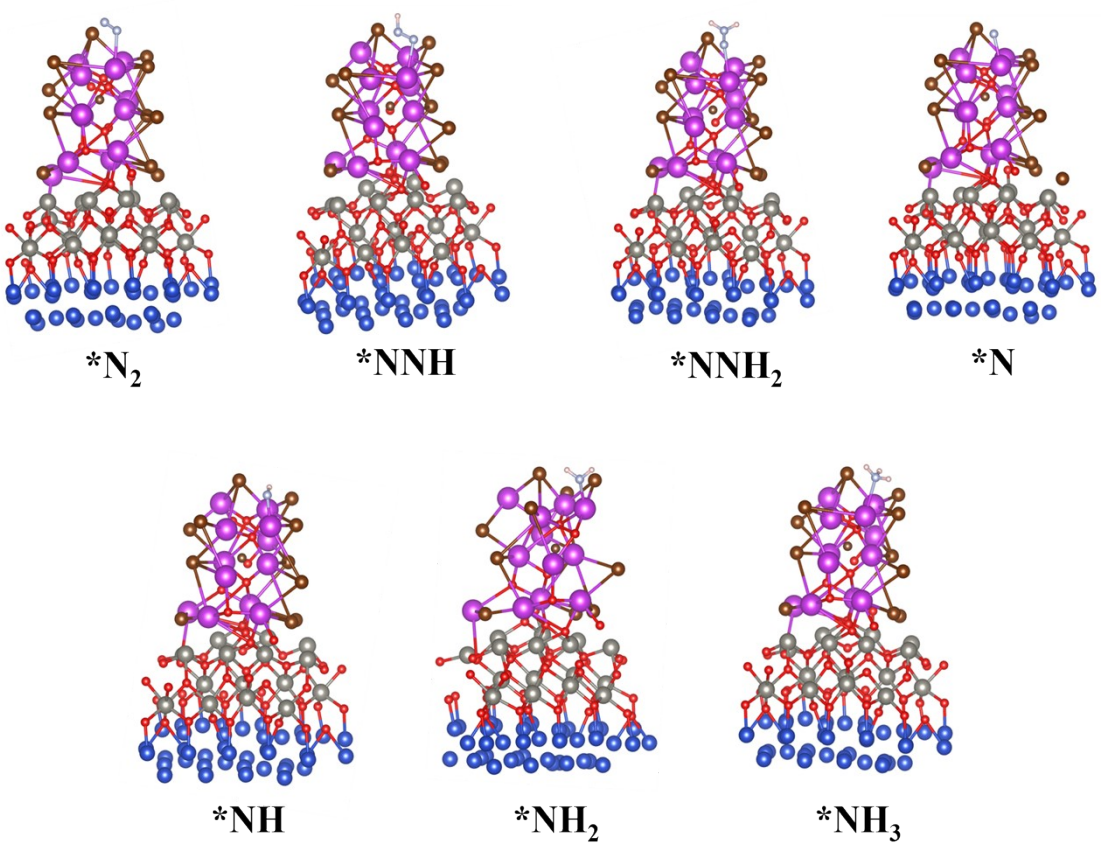

Fig. S17. The adsorption diagrams of the N_2 fixation process over Cu/WO_2/C-BOB.

Table S1. Analysis of consequence of element molar content in Cu/WO_2/C-BOB through EDS and ICP-AES.

Element		Bi	Cu	W
Molar Percentage (%)	EDS	0.71	0.26	0.15
	ICP-AES	0.74	0.28	0.19

Table S2. Oxygen vacancy peak area values for samples.

Samples	**Peak area of oxygen vacancies**
Pure BOB	2733.9
Cu/WO_2	8633.4
C-BOB	7674.1
Cu/WO_2/ C-BOB	10358.0

Table S3. Comparison of photocatalytic nitrogen fixation performance of reported bismuth-based materials.

Catalyst	**sacrificial reagent**	**NH_3 production rate ($\mu mol\ g^{-1}\ h^{-1}$)**	**Ref.**
C-BiOI	Ethanol	31.1	[5]
BiOBr/$Bi_4O_5Br_2$	None	66.87	[6]
$Bi_2O_2CO_3$ (OVs)	0.5 M Na_2SO_4 (aq)	58.9	[7]
Cu-Bi_2MoO_6	Methanol	31.4	[8]
Bi-Bi_2O_3/ $KTa_{0.5}Nb_{0.5}O_3$	Methanol	46.62	[9]
$Bi_2Sn_2O_7$ QDs	None	334.8	[10]
BSO-UNPs	None	231	[11]
$Bi_2Sn_2O_7$/BiOBr	None	459.04	[12]
BOB-001-OVs	None	223.3	[13]
Bi_2MoO_6/ OV-BiOBr	None	90.7	[14]
Vo-BiOBr	None	54.7	[15]
Pt/BOB-VO	None	23.8	[16]
Bi/BiOBr	0.025 M H_2SO_4 / 0.025 M Na_2SO_3 (aq)	55.65	[17]
Bi-Bi_2O_3/ $CdWO_4$	Methanol	43.49	[18]
OVs-$BiVO_4$	Methanol	32.4	[19]
Cu/WO_2/C-BOB	**None**	**477.5**	**This work**

References

1 Y. Sun, H. Ji, Y. Sun, G. Zhang, H. Zhou, S. Cao, S. Liu, L. Zhang, W. Li, X. Zhu, H. Pang, Synergistic effect of oxygen vacancy and high porosity of nano MIL-125(Ti) for enhanced photocatalytic nitrogen fixation. *Angew. Chem. Int. Ed.*, 2023, n/a, e202316973.

2 G. Dong, X. Huang, Y. Bi, Anchoring black phosphorus quantum dots on Fe-doped $W_{18}O_{49}$ nanowires for efficient photocatalytic nitrogen fixation. *Angew. Chem. Int. Ed.*, 2022, **61**, e202204271.

3 G. Kresse, J. Furthmüller, Efficiency of Ab-Initio total energy calculations for 34metals and semiconductors using a Plane-Wave basis set. *Comp. Mater. Sci.*, 1996, **6**, 15-50.

4 J.P. Perdew, K. Burke, M. Ernzerhof, Generalized gradient approximation made simple. *Phys. Rev. Lett.*, 1996, **77**, 3865-3868.

5 L. Zeng, F. Zhe, Y. Wang, Q.L. Zhang, X.Y. Zhao, X. Hu, Y. Wu, Y.M. He, Preparation of interstitial carbon doped BiOI for enhanced performance in photocatalytic nitrogen fixation and methyl orange degradation, *J. Colloid Interface Sci.*, 2019, **539**, 563-574.

6 H.Q. Wang, Z.H. Chen, Y.R. Shang, C.D. Lv, X.H. Zhang, F. Li, Q.Z. Huang, X.D. Liu, W.M. Liu, L. Zhao, Boosting carrier separation on a $BiOBr/Bi_4O_5Br_2$ direct Z-Scheme heterojunction for superior photocatalytic nitrogen fixation, *ACS Catal.*, 2024, **14**, 5779-5787.

7 Y. Feng, Z. Zhang, K. Zhao, S. Lin, H. Li, X. Gao, Photocatalytic nitrogen fixation: oxygen vacancy modified novel micro-nanosheet structure $Bi_2O_2CO_3$ with band gap engineering, *J. Colloid Interface Sci.*, 2021, **583**, 499-509.

8 J.F. Wang, C.R. Zhao, S.D. Yuan, X.J. Li, J.Y. Zhang, X. Hu, H.J. Lin, Y. Wu, Y.M. He, One-step fabrication of Cu-doped Bi_2MoO_6 microflower for enhancing performance in photocatalytic nitrogen fixation, *J. Colloid Interface Sci.*, 2023, **635**, 427-438.

9 L. Chen, J.F. Wang, X.J. Li, C.R. Zhao, X. Hu, Y. Wu, Y.M. He, A novel Z-scheme Bi-Bi_2O_3/$KTa_{0.5}Nb_{0.5}O_3$ heterojunction for efficient photocatalytic conversion of N_2 to NH_3, *Inorg. Chem. Front.*, 2022, **9**, 2714.

10 Y. Zhang, J. Di, X. Qian, M.X. Ji, Z.Q. Tian, L.Q. Ye, J.Z. Zhao, S. Yin, H.M. Li, J.X. Xia, Oxygen vacancies in $Bi_2Sn_2O_7$ quantum dots to trigger efficient photocatalytic nitrogen reduction, *Appl. Catal. B: Environ.*, 2021, **299**, 120680.

11 S. Gao, R.J. Wu, M.M. Sun, M. Guo, D.B. DuBois, S.W. Chen, H.D. Ji, C.Z. Wang, Q. Wang, High-performance nitrogen photofixation by $Bi_2Sn_2O_7$ nanoparticles enriched with oxygen vacancies, *Appl. Catal. B: Environ.*, 2023, **324**, 122260.

12 Y. Zhang, J. Di, X.W. Zhu, M.X. Ji, C. Chen, Y.A. Liu, L. N. Li, T.G. Wei, H.M. Li, J.X. Xia, Chemical bonding interface in $Bi_2Sn_2O_7$/BiOBr S-scheme heterojunction triggering efficient N_2 photofixation, *Appl. Catal. B: Environ.*, 2023, **323**, 122148.

13 H. Li, J. Shang, Z. Ai, L. Zhang, Efficient visible light nitrogen fixation with BiOBr nanosheets of oxygen vacancies on the exposed {001} facets, *J. Am. Chem. Soc.*, 2015, **137**, 6393-6399.

14 X. Xue, R. Chen, C. Yan, Y. Hu, W. Zhang, S. Yang, L. Ma, G. Zhu, Z. Jin, Efficient photocatalytic nitrogen fixation under ambient conditions enabled by the heterojunctions of n-type Bi_2MoO_6 and oxygen-vacancy-rich p-type BiOBr, *Nanoscale*, 2019, **11**, 10439-10445.

15 X. Xue, R. Chen, H. Chen, Y. Hu, Q. Ding, Z. Liu, L. Ma, G. Zhu, W. Zhang, Q. Yu, J. Liu, J. Ma, Z. Jin, Oxygen vacancy engineering promoted photocatalytic ammonia synthesis on ultrathin two dimensional bismuth oxybromide nanosheets, *Nano Lett.*, 2018, **18**, 7372-7377.

16 G.M. Ren, M. Shi, Z.Z. Li, Z.S. Zhang, X.C. Meng, Electronic metal-support interaction via defective-induced platinum modified BiOBr for photocatalytic N_2 fixation, *Appl. Catal. B: Environ.*, 2023, **327**, 122462.

17 Y.W. Huang, Y.S. Zhu, S.J. Chen, X.Q. Xie, Z.J. Wu, N. Zhang, Schottky junctions with Bi cocatalyst for taming aqueous phase N_2 reduction toward enhanced solar ammonia production, *Adv. Sci.*, 2021, **8**, 2003626.

18 C.R. Zhao, X.J. Li, L. Yue, S.D. Yuan, X.J. Ren, Z.H. Zeng, X. Hu, Y. Wu, Y.M. He, One-step preparation of novel Bi-Bi_2O_3/$CdWO_4$ Z-scheme heterojunctions with enhanced performance in photocatalytic NH_3 synthesis, *J. Alloys Compd.*, 2023, **968**, 171956.

19 S. Gao, R.J. Wu, M.M. Sun, M. Guo, D.B. DuBois, S.W. Chen, H.D. Ji, C.Z. Wang, Q. Wang, High-performance nitrogen photofixation by $Bi_2Sn_2O_7$ nanoparticles enriched with oxygen vacancies, *Appl. Catal. B: Environ.*, 2023, **324**, 122260.